INVERSE KINEMATIC OF A TWO-DEGREES OF FREEDOM PARALLEL MOVING PLATFORM

Cai Viet Anh Dung, Tran Quoc Dai, Le Thanh Tung*

Ho Chi Minh City University of Technology and Education, Vietnam

*Corresponding author: tunglt@hcmute.edu.vn

(Received: April 01, 2025; Revised: May 30, 2025; Accepted: June 10, 2025)

DOI: 10.31130/ud-jst.2025.23(6A).179E

Abstract - This paper presents a kinematic modeling approach for a two-degree-of-freedom (DOF) parallel mechanism moving platform. The system features a moving platform connected to the base via two Cardan joints, allowing rotation about two intersecting tilt axes (roll and pitch). Two DC motors fixed to the base drive the platform through two Revolute–Spherical–Spherical (RSS) mechanisms [1], enabling precise control of the tilt angles. A general inverse kinematics method for this and similar mechanisms is proposed and validated through experiments to evaluate the model's accuracy and effectiveness. The results demonstrate the method's applicability to the design and development of virtual reality (VR) chair systems, offering flexible two-DOF motion. This approach has potential applications in motion simulation and mechatronic system control.

Key words - Virtual reality; parallel mechanism; kinematic model

1. Introduction

Today, new developments in the field of virtual reality (VR) and force-feedback simulation have considerably enhanced immersive technology, which has become more and more accessible due to affordable computers and equipment. In this context, flight simulators have made tremendous advances. Over the last three decades, several systems have been developed and introduced to the market [2] - [4]. Combined with detailed environments and continuously improving physically simulated environments, these systems allow trainees to experience simulated sessions that closely resemble real flights [5]. While visual feedback plays a crucial role in these systems, the well-designed dynamic control of motion platforms is also essential for accurately reproducing aircraft motion [6].

Flight simulators and other motion platform simulators generally use parallel mechanisms consisting of multiple closed-loop kinematics chains that connect a moving platform to a fixed base. These mechanisms are designed to simulate the dynamic movements of an aircraft. Since the simulation of large movements is not required, they offer the advantage of lower inertia, allowing for smoother and more precise movements compared to serial-link mechanisms, while also being more compact and space-efficient [7] - [11].

Virtual reality motion platforms require real-time control to ensure that physical movements are synchronized with actions in the virtual environment. Data from sensors (such as optical encoders or IMUs) are used to measure platform movement and are sent to the VR simulator to update the virtual object's state (position/orientation) and, if necessary, determine virtual interactive forces.

Minimizing latency and improving the overall smoothness of the experience are also important. To this end, different control techniques that predict position shifts and adjust the platform's motion to reduce delay have been investigated [12], [13].

In recent years, several studies have continued to improve the design and control of motion platforms, especially Stewart-type platforms, to meet higher requirements for accuracy and response time in flight simulation [14] - [16].

In most cases, solving the inverse kinematics of the mechanism connecting the motion platform to the ground allows the determination of the platform's position and orientation, which are then sent to the simulator [17]. This paper presents a general method for determining the inverse kinematics of a motion platform, which is essential for real-time control and simulation of these systems. A prototype was built to validate this approach.

2. System design and Modeling

2.1. The mechanical design of the system

The model will include a base to support all other components. The system will use two DC motors, which are mounted onto the base component through two mounting fixtures for each motor, specifically from the perspective of the model's rear view.

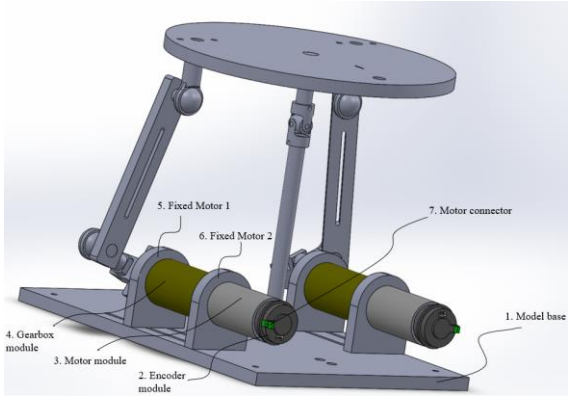

Figure 1. *Motor arrangement*

The model base (1) will be a rectangular box-shaped plate. On this base, two DC gear motors (consisting of components such as the encoder module (2), motor module (3), and gearbox module (4) in sequence from back to front) will be positioned parallel to each other along the length of the base component. Each motor will be secured using two mounting fixtures (Fixed Motor 1 (5) and Fixed

Motor 2 (6)). At the rear of the model, specifically at the back of the two motors, there will be a connection area for the control unit, which includes motor connectors (7) for motor control and encoder feedback.

2.2. Transmission system

From the perspective of the model's front view, the DC gear motor 01 (8) is placed at the left of the model and the second one (the DC gear motor 02 (9)) is placed at the right of the model. The motor-gearbox shafts are directly connected to the drive mechanism, which then transmits the motion to the moving platform (10) to adjust the tilt angles.

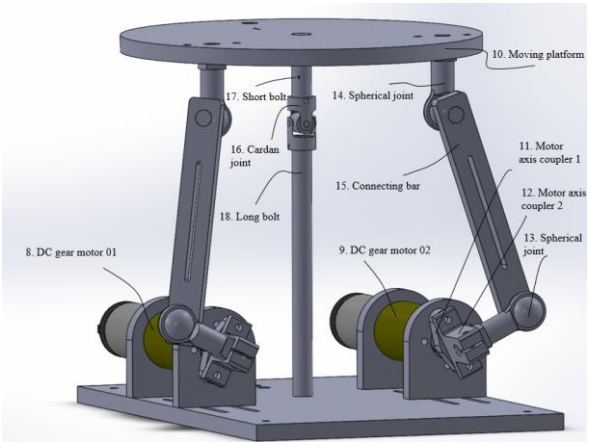

Figure 2. *The virtual chair prototype*

Specifically, the shaft of each motor will be attached to two motor axis couplers (motor axis coupler 1 (11) and motor axis coupler 2 (12)). The motor axis coupler 2 will then be connected to a spherical joint (13). The moving platform will also be equipped with two spherical joints (14) (one on each side). These spherical joints on the moving platform will be connected to the spherical joints attached to the motors via connecting bars (15). Additionally, at the center of the moving platform, a cardan joint (16) will be connected through two bolts (the short bolt (17) securing the seat base to the cardan joint and the long bolt (18) securing the cardan joint to the model's base component). This configuration ensures that as the motors rotate, the moving platform can tilt without translational movement.

2.3. Kinematic modeling

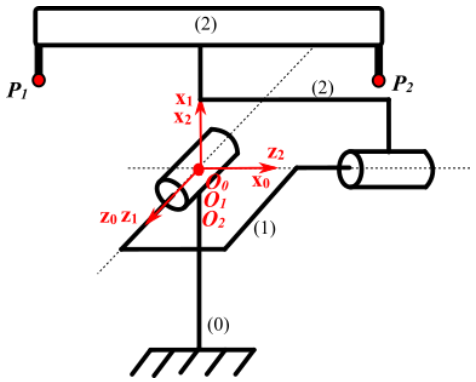

Figure 3. *Kinematic scheme of the Cardan joint*

with $(0), (1), (2)$: Links of the Cardan joint mechanism; O_0, O_1, O_2: origins of the coordinate frames attached to each link.

Table 1. *Modified D.H. parameters*

Matrix	α_i	a_i	θ_i	d_i
T_{01}	0	0	$\theta_1+\pi/2$	0
T_{12}	$\pi/2$	0	θ_2	0

The homogeneous transform matrix of the system can be defined as follows:

$$T_{01} = \begin{bmatrix} -s\theta_1 & -c\theta_1 & 0 & 0 \\ c\theta_1 & -s\theta_1 & 0 & 0 \\ 0 & 0 & 1 & 0 \\ 0 & 0 & 0 & 1 \end{bmatrix}$$

$$T_{12} = \begin{bmatrix} c\theta_2 & -s\theta_2 & 0 & 0 \\ 0 & 0 & -1 & 0 \\ s\theta_2 & c\theta_2 & 0 & 0 \\ 0 & 0 & 0 & 1 \end{bmatrix}$$

$$T_{02} = T_{01} \times T_{12} = \begin{bmatrix} -s\theta_1 c\theta_2 & s\theta_1 s\theta_2 & c\theta_1 & 0 \\ c\theta_1 c\theta_2 & -c\theta_1 s\theta_2 & s\theta_1 & 0 \\ s\theta_2 & c\theta_2 & 0 & 0 \\ 0 & 0 & 0 & 1 \end{bmatrix} \quad (1)$$

with T_{01}, T_{02}: The homogeneous transform from frame $\{0\}$ (located at the center of the cardan joint) to frame $\{1\}$ and $\{2\}$, respectively; θ_1, θ_2: The rotation angle about axes z_1 and z_2, respectively.

The coordinates of points P_1 and P_2 in (R_2 - the coordinate frame attached to the second link) are:

$$P_{1_{R_2}} = \begin{bmatrix} x_1 \\ y_1 \\ z_1 \\ 1 \end{bmatrix}; \; P_{2_{R_2}} = \begin{bmatrix} x_2 \\ y_2 \\ z_2 \\ 1 \end{bmatrix} \quad (2)$$

Now we can write the coordinates of points P_1 and P_2 in (R_0) (the coordinate frame is placed at the center of the cardan joint):

$$P_{1_{R_0}} = \begin{bmatrix} x_{P_1} \\ y_{P_1} \\ z_{P_1} \\ 1 \end{bmatrix} = T_{02} \times P_{1_{R_2}} = \begin{bmatrix} -s\theta_1 c\theta_2 x_1 + s\theta_1 s\theta_2 y_1 + c\theta_1 z_1 \\ c\theta_1 c\theta_2 x_1 - c\theta_1 s\theta_2 y_1 + s\theta_1 z_1 \\ s\theta_2 x_1 + c\theta_2 y_1 \\ 1 \end{bmatrix} \quad (3)$$

$$P_{2_{R_0}} = \begin{bmatrix} x_{P_1} \\ y_{P_1} \\ z_{P_1} \\ 1 \end{bmatrix} = T_{02} \times P_{2_{R_2}} = \begin{bmatrix} -s\theta_1 c\theta_2 x_2 + s\theta_1 s\theta_2 y_2 + c\theta_1 z_2 \\ c\theta_1 c\theta_2 x_2 - c\theta_1 s\theta_2 y_2 + s\theta_1 z_2 \\ s\theta_2 x_2 + c\theta_2 y_2 \\ 1 \end{bmatrix} \quad (4)$$

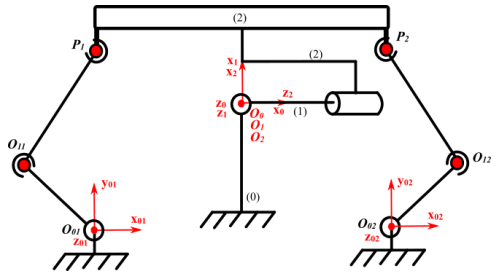

Figure 4. *Frame assignment of the whole system*

We identify the coordinates of points O_{01} and O_{02} in the base of (R_0 - the coordinate frame is placed at the center of

the cardan joint):

$$O_{01_{R_0}} = \overrightarrow{O_0O_{01_{R_0}}} = \begin{bmatrix} o_{x_1} \\ o_{y_1} \\ o_{z_1} \\ 1 \end{bmatrix};\ O_{02_{R_0}} = \overrightarrow{O_0O_{02_{R_0}}} = \begin{bmatrix} o_{x_2} \\ o_{y_2} \\ o_{z_2} \\ 1 \end{bmatrix} \quad (5)$$

Next we write the homogeneous transform matrix $T_{01\text{-}0}$ between (R_{01} - the coordinate frame is placed at the motor axis coupler 2 attached to the DC gear motor 01) and (R_0) and the homogeneous transform matrix $T_{02\text{-}0}$ between (R_{02} - the coordinate frame is placed at the motor axis coupler 2 attached to the DC gear motor 02) and (R_0):

$$T_{01-0} = \begin{bmatrix} 1 & 0 & 0 & -o_{x_1} \\ 0 & 1 & 0 & -o_{y_1} \\ 0 & 0 & 1 & -o_{z_1} \\ 0 & 0 & 0 & 1 \end{bmatrix};\ T_{02-0} = \begin{bmatrix} 1 & 0 & 0 & -o_{x_2} \\ 0 & 1 & 0 & -o_{y_2} \\ 0 & 0 & 1 & -o_{z_2} \\ 0 & 0 & 0 & 1 \end{bmatrix} \quad (6)$$

Then we can write the coordinates of points P_1 and P_2 in the bases of *(R_{01})* and *(R_{02})*:

$$P_{1_{R_{01}}} = T_{01-0} \times P_{1_{R_0}} = \begin{bmatrix} x_{P_1} - o_{x_1} \\ y_{P_1} - o_{y_1} \\ z_{p_1} - o_{z_1} \\ 1 \end{bmatrix} = \begin{bmatrix} x_{P_{11}} \\ y_{P_{11}} \\ z_{P_{11}} \\ 1 \end{bmatrix} \quad (7)$$

$$P_{2_{R_{02}}} = T_{02-0} \times P_{2_{R_0}} = \begin{bmatrix} x_{P_2} - o_{x_2} \\ y_{P_2} - o_{y_2} \\ z_{p_2} - o_{z_2} \\ 1 \end{bmatrix} = \begin{bmatrix} x_{P_{22}} \\ y_{P_{22}} \\ z_{P_{22}} \\ 1 \end{bmatrix} \quad (8)$$

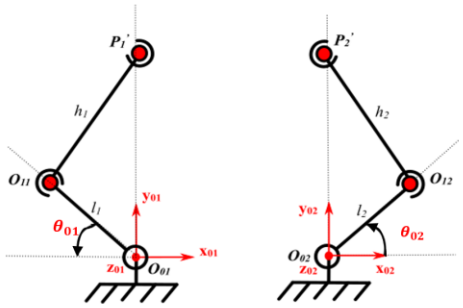

Figure 5. *Projections of the mechanical linkages onto the planes*

Next we have to define the coordinates of point P_1' and P_2' in the base of (R_{01}) and (R_{02}) by simply projecting the points P_1 and P_2 onto the planes (x_{01}. y_{01}) i.e. by putting the z coordinates of the 2 points to zero.

$$P'_{1_{R_{01}}} = \begin{bmatrix} x_{P_{11}} \\ y_{P_{11}} \\ 0 \\ 1 \end{bmatrix};\ P'_{2_{R_{02}}} = \begin{bmatrix} x_{P_{22}} \\ y_{P_{22}} \\ 0 \\ 1 \end{bmatrix} \quad (9)$$

The distances between O_{11} and P_1 as well as the distances between O_{12} and P_2 are equal to a constant distance r. We can thus determine the distances $O_{11}P_1' = h_1$ and $O_{12}P_2' = h_2$ using Pythagorean formula:

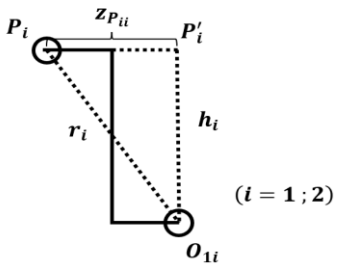

Figure 6. *Determine the distance h*

$$h_1 = \sqrt{r^2 - z_{P_{11}}^2};\ h_2 = \sqrt{r^2 - z_{P_{22}}^2} \quad (10)$$

From this point, all the parameters are available to reduce the problem to the inverse kinematics of a 2-degree-of-freedom robotic arm mechanism. This allows the calculation of the motor rotation angles corresponding to different tilt angles of the seat base component.

Specifically, the research team chose to solve the inverse kinematics problem using the geometric method. This approach enables a direct analytical solution (closed-form), which is computationally efficient and suitable for real-time control. Compared to matrix-based or iterative numerical algorithms, the geometric method reduces calculation time and minimizes errors accumulated through iterative processes.

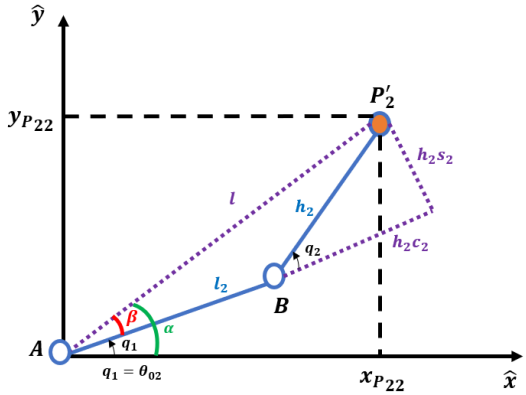

Figure 7. *Inverse kinematics using the geometric method to find the angle θ_{02}*

From the previous steps, we have obtained the following parameters:

$$\begin{cases} l_2 \\ h_2 \\ l = \sqrt{x_{P_{22}}^2 + y_{P_{22}}^2} \\ q_1 = \theta_{02} \end{cases} \quad (11)$$

with l: the distance between O_{02} and P_2' l_2: the length of link 1; h_2: the length of link 2; q_1: the angle between link 2 and x-axis; θ_{02}: the motor 2 rotation angle.

The angle we need to find here is the angle q_1 (which is the motor rotation angle θ_{02} that needs to be determined.

We have the following formula:

$$\theta_{02} = q_1 = \alpha - \beta \quad (12)$$

We can find the values of the two angles α and β as follows:

$$\begin{cases} \alpha = atan2(y_{P_{22}}, x_{P_{22}}) \\ \beta = atan2(h_2 s_2, l_2 + h_2 c_2)\ (với\ c_2 = \cos(q_2)) \end{cases} \quad (13)$$

Where the values of $x_{P_{22}}$ and $y_{P_{22}}$ have been determined from the previous steps. What we need to do now is to find the values of c_2 and s_2 ($\cos(q_2)$ and $\sin(q_2)$). We will determine c_2 first as follows: According to the law of cosines in triangle $\Delta ABP_2'$, we get:

$$l^2 = l_2^2 + h_2^2 - 2l_2h_2\cos(180 - q_2) \quad (14)$$

$$x_{P_{22}}^2 + y_{P_{22}}^2 = l_2^2 + h_2^2 + 2l_2h_2\cos(q_2) \quad (15)$$

$$c_2 = \frac{\left(x_{P_{22}}^2 + y_{P_{22}}^2\right) - \left(l_2^2 + h_2^2\right)}{2 l_2 h_2} \; with \; (\cos(q_2) = c_2) \quad (16)$$

After obtaining c_2, we will continue to find s_2 using the trigonometric identity:

$$s_2^2 + c_2^2 = 1 \quad (17)$$

$$s_2 = \pm\sqrt{1 - c_2^2} \quad (17)$$

Thus, after solving the inverse kinematics problem using the geometric method, we can find the desired motor rotation angle θ_{02} as follows:

$$\theta_{02} = q_1 = \alpha - \beta$$

$$\theta_{02} = atan2(y_{P_{22}}, x_{P_{22}}) - atan2(h_2 s_2, l_2 + h_2 c_2) \quad (19)$$

Next, we will fine θ_{01} as follow:

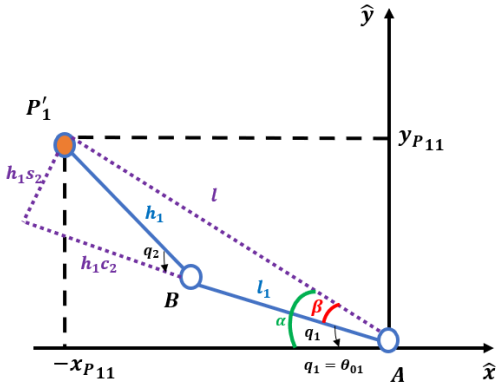

Figure 8. *Inverse kinematics using the geometric method to find the angle* θ_{01}

Here, we have also determined several parameters from the previous step:

$$\begin{cases} l_1 \\ h_1 \\ l = \sqrt{x_{P_{11}}^2 + y_{P_{11}}^2} \\ q_1 = \theta_{01} \end{cases} \quad (20)$$

with l: the distance between O_{02} and P_2'; l_1: the length of link 1; h_1: the length of link 2; q_1: the angle between link 2 and the negative x-axis; θ_{01}: the motor 1 rotation angle

The steps to calculate θ_1 will be almost similar to those used for calculating θ_2, but with a slight difference: we will use the negated value of $x_{P_{11}}$ and when calculating the final value of θ_1, we will add a negative sign to the result obtained. Specifically, the calculation steps are as follows:

Firstly, as mentioned, we will take the negated value of $x_{P_{11}}$ and store it in a new variable called $x_{P'_{11}}$.

$$x_{P'_{11}} = -x_{P_{11}} \quad (21)$$

Thus, by using the negated value of $x_{P_{11}}$, the angles α and β will align correctly as illustrated in the diagram above. The angle we need to determine here is q_1, which is precisely the motor rotation angle θ_1 we are looking for.

To maintain the positive direction of θ_{01} following the right-hand rule (similar to θ_2), the calculation will proceed in the same manner, but a negative sign will be added to the final result:

$$\theta_{01} = q_1 = -(\alpha - \beta) \quad (22)$$

The values of the two angles α and β are determined as follows:

$$\begin{cases} \alpha = atan2(y_{P_{11}}, x_{P'_{11}}) \\ \beta = atan2(h_1 s_2, l_1 + h_1 c_2) \; (với \; c_2 = \cos(q_2)) \end{cases} \quad (23)$$

Where the values of $x_{P_{11}}$ and $y_{P_{11}}$ have been determined from the previous steps. What we need to do now is to find the values of c_2 and s_2 ($\cos(q_2)$ and $\sin(q_2)$). We will determine c_2 first as follows: According to the law of cosines in triangle $\Delta ABP_2'$, we get:

$$l^2 = l_1^2 + h_1^2 - 2 l_1 h_1 \cos(180 - q_2) \quad (24)$$

$$x_{P_{11}}^2 + y_{P_{11}}^2 = l_1^2 + h_1^2 + 2 l_1 h_1 \cos(q_2) \quad (25)$$

$$c_2 = \frac{\left(x_{P'_{11}}^2 + y_{P_{11}}^2\right) - \left(l_1^2 + h_1^2\right)}{2 l_1 h_1} \; (\cos(q_2) = c_2) \quad (26)$$

After obtaining c_2, we will continue to find s_2 using the trigonometric identity:

$$s_2^2 + c_2^2 = 1 \quad (27)$$

$$s_2 = \pm\sqrt{1 - c_2^2} \quad (28)$$

Thus, after solving the inverse kinematics problem using the geometric method, we can find the desired motor rotation angle θ_{01} as follows:

$$\theta_{01} = q_1 = -(\alpha - \beta) \quad (29)$$

$$\theta_{01} = -\left(atan2(y_{P'_{11}}, x_{P_{11}}) - atan2(h_1 s_2, l_1 + h_1 c_2)\right) \quad (30)$$

3. Control solution

Figure 9 illustrates the control solution of the system. The desired tilt angle of the model will be input into the computer, which will then calculate the two motor rotation angles based on the kinematic formulas presented above.

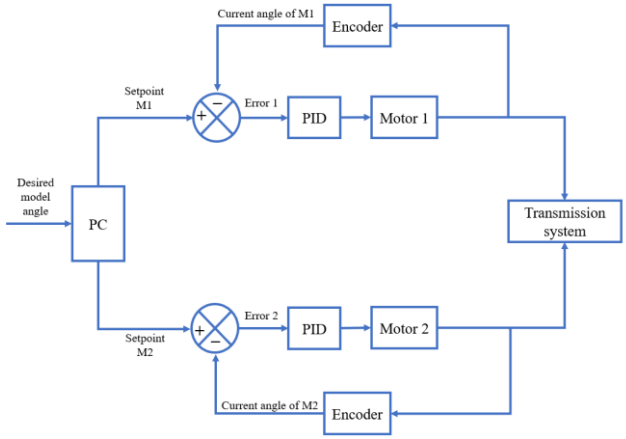

Figure 9. *The system control scheme*

From that, each motor will have a specific target rotation angle, which will be compared with the current rotation position measured by the encoder installed in each motor. This allows us to compute the deviation and feed this value into the PID controller to control the motor's rotation.

The motor's rotation will affect the mechanism, transmitting motion to the seat base and causing it to tilt according to the desired angle initially entered into the computer.

In this system, the motors are coupled with high-ratio gearboxes due to the application's requirement for high torque rather than high speed. As a result of the large gear

ratio and the relatively low operating speed, the overall system inertia remains small. This characteristic simplifies the tuning process of the PID controller.

The tuning process began by determining suitable values of K_p and K_d to ensure a fast response with minimal overshoot and acceptable steady-state error. Once these values were set, the integral gain K_i was introduced to further reduce the steady-state error. However, the inclusion of the integral term caused small oscillations around the setpoint, especially when the system approached convergence. To address this, K_p was slightly reduced, and a constraint was added to the control output: when the steady-state error fell below 0.1°, the PWM signal was forced to 0%. This prevented the controller from applying small corrective actions that could lead to persistent oscillations due to the integral effect.

Through this tuning method, the system achieved a fast and stable response with minimal steady-state error. The final controller parameters selected for the system were:

- Proportional gain $K_p = 7.4$;
- Integral gain $K_i = 12.76$;
- Derivative gain $K_d = 0.17$.

Through this tuning approach, the research team aimed to achieve minimal steady-state error while maintaining fast dynamic response, thereby demonstrating the effectiveness of a carefully tuned PID controller in systems characterized by low inertia and high transmission ratios.

4. Result and Discussion

Figure 10 presents the first prototype of 2 d.o.f. VR chair. The two motors will be fixed underneath the base of the entire model. The output shaft of each motor will be coupled with two shaft support components to connect to a single spherical joint. The moving platform on top will also be equipped with a spherical joint on each side. Thus, the spherical joint on each side of the moving platform will be connected to the corresponding spherical joint attached to the motor via a connecting bar.

Figure 10. Prototype of the 2 d.o.f. moving platform

An experiment was conducted by selecting four tilt positions in sequence and inputting them into the computer. These values were then used to calculate the desired set-points for the rotation angles of each motor. The moving platform was controlled to sequentially move through the four tilt positions, pausing for approximately a half of second at each desired tilt position to allow the system to stabilize before transitioning to the next position. During the experiment, an accelerometer is mounted on a board that is fixed to the underside of the moving platform (Figure 11). This sensor was used to measure the tilt angles of the moving platform (the measurements served only for verification and did not influence the control process). The data displayed on the graph included the set-points for the motor rotation angles, the response process of the motors to achieve these set-points, and the tilt angles of the moving platform.

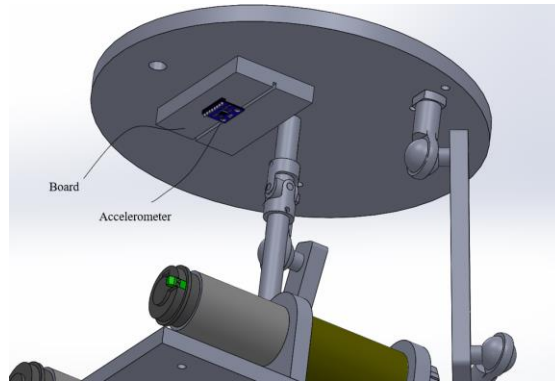

Figure 11. *Accelerometer placement*

The four tilt positions of the model correspond to the following set-points for the rotation angles of the two motors:

First position:

$$\begin{cases} Roll = \theta_1 = 20° \\ Pitch = \theta_2 = 0° \end{cases} \rightarrow \begin{cases} \theta_{01} = 11° \\ \theta_{02} = 52° \end{cases}$$

Second position:

$$\begin{cases} Roll = \theta_1 = 0° \\ Pitch = \theta_2 = -25° \end{cases} \rightarrow \begin{cases} \theta_{01} = -42° \\ \theta_{02} = 42.4° \end{cases}$$

Third position:

$$\begin{cases} Roll = \theta_1 = -20° \\ Pitch = \theta_2 = 0° \end{cases} \rightarrow \begin{cases} \theta_{01} = -49.6° \\ \theta_{02} = -12° \end{cases}$$

Fourth position:

$$\begin{cases} Roll = \theta_1 = 0° \\ Pitch = \theta_2 = 20° \end{cases} \rightarrow \begin{cases} \theta_{01} = -0.2° \\ \theta_{02} = 0.7° \end{cases}$$

The results indicate that, with the PID controller, the motor response performs well with a steady-state error remaining ($\leq 0.1°$). However, occasional minor overshoots still occurred ($\leq 0.5°$). Regarding the accuracy of the model's tilt position, as measured by the accelerometer sensor, the total error for both the roll and pitch angles is $\leq 5°$. However, the results obtained from the accelerometer may not be highly reliable, as they are influenced by various external factors. These include sensor inaccuracies, mechanical uncertainties inherent in the structure, and potential misalignment or instability in sensor mounting during operation.

To provide a clearer understanding of the system scale and technical parameters, Table 2 summarizes key specifications, including physical dimensions, mass, tilt angle range. The system is built at approximately a 1:4 scale compared to a full-sized VR chair, serving primarily as a mechanical training model. While this study focuses on kinematics and control implementation, practical applications will require further consideration of dynamics, load capacity, structural strength, safety standards, and realistic transmission solutions, which are critical for developing a commercial VR chair.

Table 2. *System Technical Specifications*

No.	Parameter	Specification
1	Dimensions (L×W×H)	30 cm × 27 cm × 26 cm
2	Scale Ratio	1:4
3	System Mass	3.9 kg
4	Tilt Angle Range	±25°
5	Estimated Load Capacity	8 kg

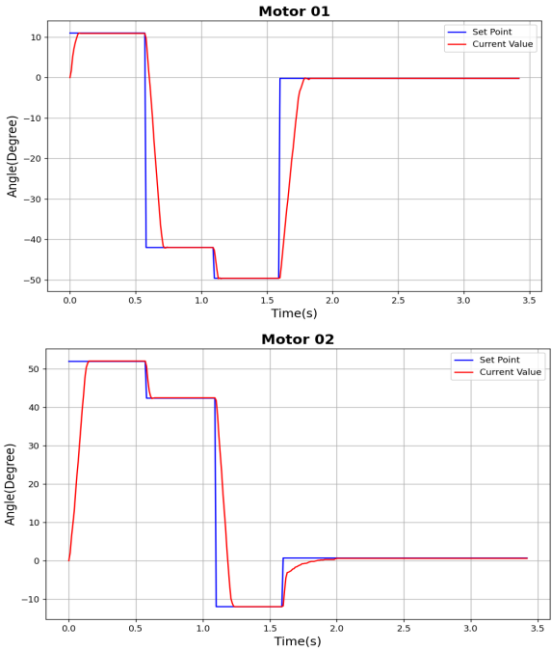

Figure 12. *The motor rotation angles*

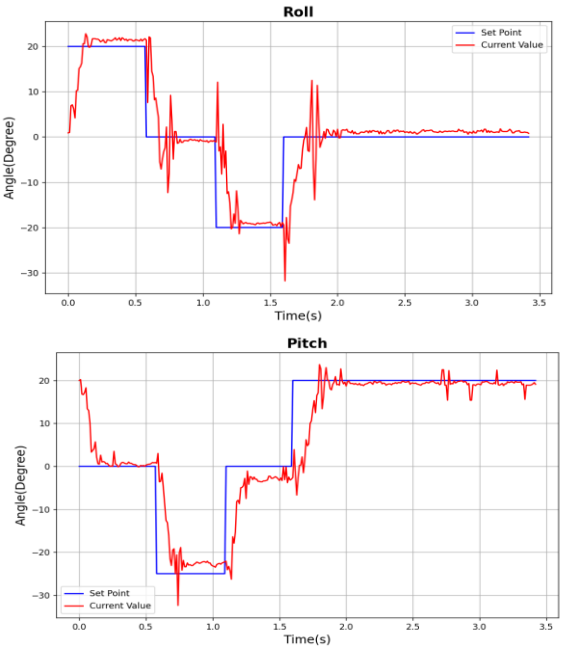

Figure 13. *The tilt angles of the moving platform*

5. Conclusions

In this paper, we present a general method for the determination of inverse kinematics of parallel motion platforms that are used in Virtual Reality. The first experiments demonstrate the ability of the system to follow changes in the reference trajectory in real time although response latency exists. The result shows the potential for using this approach to build human-scale VR chairs. Unlike previous studies that primarily focused on theoretical models or simulations, this work emphasizes the practical implementation of a 2-DOF parallel mechanism, featuring real-time control and sensor-based feedback. Predictive control algorithms should be investigated in the future in order to improve the smoothness of the platform motion when the latter is in interaction with the VR simulator.

REFERENCES

[1] L. W. Tsai, *The Mechanics of Serial and Parallel Manipulators*, 1st edition. John Wiley & Sons, 1999.

[2] H. Gu, D. Wu, and H. Liu, "Development of a Novel Low-Cost Flight Simulator for Pilot Training", *World Academy of Science - Engineering and Technology International Journal of Computer and Systems Engineering,* vol. 3, no. 12, 2009.

[3] J. B. Cohen, N. N. Soja, and T. Longridge, "Simulator Platform Motion - The Need Revisited", *The International Journal of Aviation Psychology,* vol. 8, no. 3, pp. 293-317,1998.

[4] A. S. J. Van Heerden, R. Lidbetter, L. Liebenberg, E. H. Mathewsb, and J. P. Meyerc, "Development of a motion platform for an educational flight simulator", *International Journal of Mechanical Engineering Education,* vol. 39, no. 4, 2011.

[5] F. Jentsch and M. Curtis, *Simulation in aviation training,* 1st edition. London: Routledge, 2017.

[6] M. Baarspul, "A review of flight simulation techniques", *Progress in Aerospace Science,* vol. 27, pp. 1-120, 1990.

[7] N. A. Pouliot and C. M. Gosselin, "Motion Simulation Capabilities of Three-Degree-of-Freedom Flight Simulators", *Journal of Aircraft*, vol. 35, no. 1, 1998.

[8] J. Kim, Y. M. Cho, F. C. Park and J. M. Lee, "Design of a Parallel Mechanism Platform for Simulating Six Degrees-of-freedom General Motion Including Continuous 360-degree Spin", *CIRP Annals,* vol. 52, no. 1,pp. 347-350, 2003.

[9] O. Schulzyk, J. Bongartz, T. Bildhauer, U. Hartmann, B. Goebel, R. Herpers, and D. Reinert, "A Bicycle Simulator Based on a Motion Platform in a Virtual Reality Environment – FIVIS Project", *Advances in Medical Engineering*, vol 114, pp. 323-328, 2007.

[10] B. Hament, A. Cater, and P. Y. Oh, "Coupling virtual reality and motion platforms for snowboard training", in *2017 14th International Conference on Ubiquitous Robots and Ambient Intelligence (URAI)*, Jeju, South Korea, 2017, pp. 556-560.

[11] F. Holzapfel, I. Sturhan, and G. Sachs, "Pilot – in – the – loop flight simulation – A low cost approach", in *AIAA Modeling and Simulation Technologies Conference and Exhibit*, Providence, Rhode Island, 2004.

[12] W. Dongsu and G. Hongbin, "Adaptive Sliding Control of Six-DOF Flight Simulator Motion Platform", *Chinese Journal of Aeronautics,* vol. 20, pp. 425-433, 2007.

[13] S. M. Lee, K. Xia, and H. Son, "Robust Tracking Control of Spherical Motion Platform for Virtual Reality", *IEEE Transactions on Industrial Electronics,* vol. 68, no. 1, pp. 892-901, 2021.

[14] M. D. Petrašinović, A. M. Grbovic, D. M. Petrašinović, M. G. Petrovic, and N. G. Raicevic, "Real Coded Mixed Integer Genetic Algorithm for Geometry Optimization of Flight Simulator Mechanism Based on Rotary Stewart Platform", *Applied Sciences*, vol. 12, no. 14, pp. 14-17, 2022.

[15] T. Liu, H. Lou, and H. Huang, "Optimal design and verification of the 6-DOF Stewart structure used in vehicle-mounted automatic assembly", in *The 6th International Conference on Mechanical, Electric, and Industrial Engineering*, Sanya, China, 2023, pp. 1-6.

[16] P. V. Lukianov and V. V. Kabanyachyi, "Mathematical model of stable equilibrium operation of the flight simulator based on the Stewart platform", *Aviation*, vol. 27, no. 2, pp. 119-128, 2023.

[17] R. L. Williams II and B. H. Shelly, "Inverse Kinematics for Planar Parallel Manipulator", *ASME Design Technical Conferences*, vol. 2, 1997.